Oxygen vacancies, the optical band gap (E_g) and photocatalysis of hydroxyapatite: Comparing modelling with measured data

V.S. Bystrov [a], C. Piccirillo [b], D.M. Tobaldi [c], P.M.L. Castro [b], J. Coutinho [d], S. Kopyl [c], R.C. Pullar [c],*

[a] Institute of Mathematical Problems of Biology RAS − Branch of Keldysh Institute of Applied Mathematics of Russian Academy of Sciences (KIAM RAS), IMPB RAS, 1 Vitkevicha str., Pushchino, 142290, Moscow District, Russia
[b] CBQF − Centro de Biotecnologia e Química Fina − Laboratório Associado, Escola Superior Biotecnologia, Universidade Católica Portuguesa, 4202-401 Porto, Portugal
[c] Department of Engineering of Materials and Ceramics/CICECO−Aveiro Institute of Materials, University of Aveiro, 3810-193 Aveiro, Portugal
[d] Department of Physics and I3N, University of Aveiro, 3810-193 Aveiro, Portugal

ARTICLE INFO

ABSTRACT

Hydroxyapatite ($Ca_{10}(PO_4)_6(OH)_2$, HAp) is a calcium phosphate employed both in biomedicine and for environmental remediation. It is known that HAp can also be photocatalytic under UV light, probably due to oxygen deficiencies, but the mechanism is unclear, and reported optical band gap energies vary greatly. For the first time we propose the mechanisms and precise kinds of vacancies which may cause the photocatalytic activity of HAp, and compare these theoretical data with our measured data on both samples of marine origin and commercial HAp powders. Density functional theory (DFT) (from first principles calculations and Density of States (DOS) modelling) was used to calculate the optical band gap energy (E_g) created by various possible oxygen vacancies in the HAp lattice: O from PO_4, O from OH, the loss of an entire OH group, or the simultaneous loss of O from PO_4 and an entire OH group. The modelled values match the measured values very closely, suggesting that in non-photocatalytic HAp, if any vacancies exist, they are O atoms from the OH group, resulting in a band gap of ∼5 eV in the UVC region (not present in solar light at the Earth's surface). However, in photocatalytic HAp, reduction from the combustion of an organic component at 1000 °C led to oxygen deficiency in the phosphate groups, probably in the O15 position, giving an E_g of ∼3.45 eV, in the UVA region (present in sunlight). Heating HAp with no organic component to 1200 °C also led to vacancies, of both an entire OH group and oxygen from PO_4 groups, which led to an intermediate E_g value of ∼4 eV, on the boundary of the UVA-UVB regions. Absorption peaks were also predicted in the visible-light region with some types of vacancy.

© 2016 Elsevier B.V. All rights reserved.

1. Introduction

Pollution of the environment is one the key challenges for our modern industrial society; the increasing level of toxic compounds, both in air and waters, requires effective methods and techniques for their degradation and/or conversion into harmless species [1]. Photocatalysis is an important methodology for environmental remediation; through which it is possible to degrade hazardous chemicals both in liquid and in the gas phase [1,2].

Photocatalysts are semiconductors, i.e. materials with an energy band gap (E_g). When irradiated with energy ≥ E_g, a negatively charged electron (e^-) can be promoted to the conduction band from the valence band; this leads to the formation of a positively charged hole (h^+) in the valence band. These two charged species can react with molecules adsorbed on the surface of the material, and such reactions can eventually lead to the degradation of these molecules [3]. Examples of the degraded molecules include dyes and pharmaceuticals in the liquid phase, while species such as nitrogen oxides (NOx), volatile organic compounds (VOCs) and alcohols/alkanes can be decomposed in the gaseous phase [4].

Beyond being used for pollution degradation, photocatalysts can also be employed for bacteria inactivation. Microorganisms can be killed by interactions with the e^-/h^+ couple or with other Reactive Oxygen Species (ROS), such as radicals, which are generated with light irradiation [5].

Table 1
Unit cell parameters a,b,c [Å] (from [31]).

Phase	Group	a, Å	b, Å	c, Å
Hexagonal	$P6_3/m$	9.417	9.417	6.875
Monoclinic	$P2_1/b$	9.48	18.96	6.83
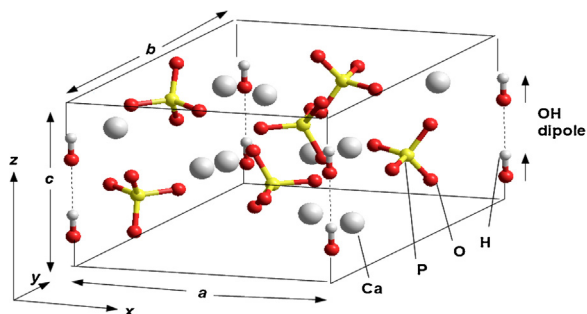
Fig. 1. Hexagonal HAp unit cell ordered structure. All OH groups are oriented in the same direction. They are positioned at the four corners of the unit cell, but only one pair in one corner belongs to this unit cell, the other three pairs belonging to neighbouring unit cells (e.g., one OH per unit cell).

Hydroxyapatite ($Ca_{10}(PO_4)_6(OH)_2$, HAp) is a calcium phosphate employed both in biomedicine and for environmental remediation. Its use in biomedicine as a material for bone implants is due to its high biocompatibility and bioactivity [6]. In environmental remediation, HAp can be used for heavy metals absorption and removal, especially for bivalent cations such as Pb (II), Cd (II) and Zn (II) [7].

In recent years, the use of HAp as a photocatalyst has also been investigated, and several studies reported some forms of HAp as being photocatalytically active. Biphasic HAp-TiO$_2$ materials, for instance, showed greater photocatalytic activity compared to either single phase HAp or TiO$_2$ [8,9]; titanium-doped HAp has also exhibited photocatalytic behaviour; in the latter case, the insertion of the Ti^{4+} ion into the HAp lattice led to light absorption in the UV region, with the absorption being stronger for higher Ti^{4+} concentrations [10,11]. Different band gap values were measured for Ti-doped HAp; generally they were between 3.0 and 3.2 eV (around the values for anatase and rutile TiO$_2$) [12], and higher values up to 3.65 eV were also measured [13].

Some forms of single-phase HAp, with no dopant, also showed photocatalytic activity; indeed, Nishikawa reported the degradation of pollutants such as methyl mercaptane and dimethyl sulphate by HAp under UV irradiation [14,15]. Some HAp of natural origin has also exhibited photocatalytic behaviour – HAp derived from both cod fish bones and mussel shells has been used to degrade methylene blue [16,17].

Despite these interesting results, however, it is not yet clear which are the structural features affecting and/or imparting the photocatalytic behaviour to some forms of HAp. According to Nishikawa, UV irradiation can lead to an oxygen vacancy in the HAp lattice. This causes an electron transfer from the HAp vacancy to the atmospheric oxygen which, in turn, leads to the formation of the charged $O_2{}^{\bullet-}$ species, and indeed, $O_2{}^{\bullet-}$ was observed with EPR spectroscopy [14,18]. $O_2{}^{\bullet-}$ can then react with liquid/gaseous molecules and degrade them.

Although the detection of $O_2{}^{\bullet-}$ can be linked to the photocatalytic activity of HAp, it does not explain why some HAp forms are photocatalytic while others are not, i.e. why some forms can generate $O_2{}^{\bullet-}$ when irradiated while others do not. Piccirillo et al., for instance, made two single-phase HAp materials from cod fish bones; of these two, only one showed photocatalytic activity, while the other did not [16]. According to the authors, a possible explanation for such a difference was the existence of an oxygen vacancy

present in the photoactive HAp material, whose formation was due to the more reducing environment the material was prepared in.

In this work we present a density functional theory (DFT) modelling study of HAp, which correlates various possible oxygen vacancies in the HAp lattice (in PO$_4$, OH, and PO$_4$ + OH sites) with the variations in the value of the optical band gap E$_g$. To achieve this, first principles calculations of the HAp lattice and Density of States (DOS) modelling of defects in this system, specifically oxygen vacancies, were used [19]. The modelling results are compared with the band gap (E$_g$) values measured by the authors in actual HAp samples, of both marine origin and commercial products, using the Tauc plot method [20].

2. Materials and methods

2.1. Sample preparation

The preparation of HAp samples of marine origin was as previously described [16]. Briefly, the clean and dried cod fish bones were treated in solution containing an excess of either calcium chloride or calcium acetate (samples indicated with the symbols **B_Ac** and **B_Cl** respectively). After the solution treatment, the bones were dried and calcined at temperatures of 1000 °C (**B_Ac_1000** and **B_Cl_1000**) or 1200 °C (**B_Cl_1200**), using a heating rate of 5 °C/min and an annealing time of 1 h. Commercial HAp samples (Biotal, samples indicated by the letter **C**) were also studied as comparison; the powder was analysed as purchased (**C**) and after annealing at 1200 °C (**C_1200**), using the same conditions described above. Previous analysis of these samples showed that they all were single-phase HAp [21].

2.2. UV spectra measurement and band gap calculation

UV–vis spectra were acquired using a Shimadzu UV 3100 JP spectrometer equipped with an integrating sphere made of BaSO$_4$, in the range 250–825 nm, with a 0.2 nm in resolution. BaSO$_4$ was used as a white reference material. To calculate the optical band gap values, the Kubelka–Munk function [22] was applied with the aim of converting the diffuse reflectance into the absorption coefficient α:

$$\alpha \approx \frac{K}{S} = \frac{(1-R_\infty)^2}{2R_\infty} \equiv F(R_\infty) \tag{1}$$

In Eq. (1) K and S are the absorption and scattering coefficients, respectively, whilst the reflectance R_∞ is equal to: $R_{sample}/R_{standard}$ [22]. Afterwards, the Tauc plot was applied [20]. This method assumes that the absorption coefficient α in (1) can be expressed as follows:

$$(\alpha h\nu)^\gamma = A(h\nu - E_g) \tag{2}$$

where A is a material constant, h is the Planck's constant, is the frequency of the light, E_g is the (optical) energy band gap of the allowed transitions, and γ is the power coefficient, characteristic for the type of transition. For HAp the value of γ is accepted to be equal to 1/2 because for such materials, the transition is assumed to be indirectly allowed [23]. So, by plotting $[F(R_\infty)h\nu\nu]^{1/2}$ against $h\nu$, we can estimate the optical E_g of the material from the x-axis ($\alpha = 0$) intercept of the line that is tangent to the inflection point of the curve. This was found by fitting the transformed Kubelka–Munk equation versus the photon energy with a sigmoidal Boltzmann function. The optical E_g value was then obtained from the x-axis intercept of the line that is tangent to the inflection point of said curve.

2.3. Modelling and computation

In this work we report density functional theory (DFT) calculations [24,25] within the local density approximation (LDA) [26] using the AIMPRO code [27–29], which is particularly suitable for the exploration of the infinite periodic crystal lattice structure of HAp [19]. This method also involves the pseudo-potential approach to avoid explicit treatment of core states [30]. For this purpose, we used standard valence configurations for the following atoms, from which the HAp unit cell is made: hydrogen ($1s^1$), phosphorus ($3s^23p^3$) and oxygen ($2s^22p^4$). For calcium atoms, we use a two-electron valence configuration ($4s^2$). The valence states were expressed as linear combinations of atom-centered Cartesian Gaussian functions, namely Ca(6,18,0), P(4,12,12), O(4,12,12), H(4,12,0), where triplets (n_s, n_p, n_d) indicate the number of independent primitive functions with s-, p- and d-like shapes for each species. The charge density and potential terms were Fourier-transformed using plane waves, with a cut-off energy of E_{cut} = 300 a.u., and the Brillouin-zone was sampled at special **k**-point grids (see below), whose density was tested previously in order to make sure that convergence of the total energy was attained [19].

The calculated optimized equilibrium HAp unit cell parameters were a = b = 9.4732 Å and c = 6.9989 Å for the hexagonal P6$_3$/m phase [19]. These compare fairly well with the experimental data [31] (see data in Table 1 for a more detailed comparison with some other calculations, and also see Table 4 in [19]), and are used in this work for the following calculation of the stoichiometric HAp lattice, and as an initial state for the defect HAp structures, particularly with O vacancies.

The initial lattice unit cell for the hexagonal HAp structure used in this work, Ca$_{10}$(PO$_4$)$_6$(OH)$_2$, consists of 44 atoms (see also Table S1 in Supplementary materials in [19]). Fig. 1 shows the initial stoichiometric HAp unit cell, with the a-axis in the hexagonal plane (space group P6$_3$/m). The hexagonal lattice was constructed to investigate the initial stoichiometric HAp structure, as well for defects in the HAp unit cell, using the HyperChem package for molecular modelling [32], similar to that used previously by the authors [19,33]. All atom positions were allowed to relax along the forces acting upon them, until the total energy converged below 10^{-5} eV. For the unit cell with 44 atoms we used a k1×k2×k3 grid of **k**-points, following the method proposed by Monkhorst and Pack [34]. All **k**-point sets were folded according to the symmetry of the problem. After several series of calculations, the standard Monkhorst–Pack **k**-point meshes for the Brillouin Zone (BZ) integration of hexagonal primitive unit cells were found to be best with 2 × 2 × 4.

Full relaxation of the cell (including changes in cell shape, cell volume and atomic positions), was carried out. The optimized data obtained for each HAp structure were taken (files with optimized and fixed coordinates for all unit cell atoms in atomic and Cartesian units were used) and converted to the HyperChem (*.hin) format (using the Babel program). Then we fed these atomic coordinate the into HyperChem software tools for further molecular modelling (with visual options for all studied HAp structures), calculations and exploration of its physical properties.

To construct the oxygen vacancy defects we used three main models:

1) Delete an O atom from the OH group in the columnar (OH-channels) structure;
2) Delete an entire OH group;
3) Delete the O atom from a PO$_4$ group.

The "OH channels" are the columns of aligned OH groups along the corners of each hexagonal HAp unit cell. These are oriented "up" or "down" along the c-axis to form an OH dipole, with the neigh-
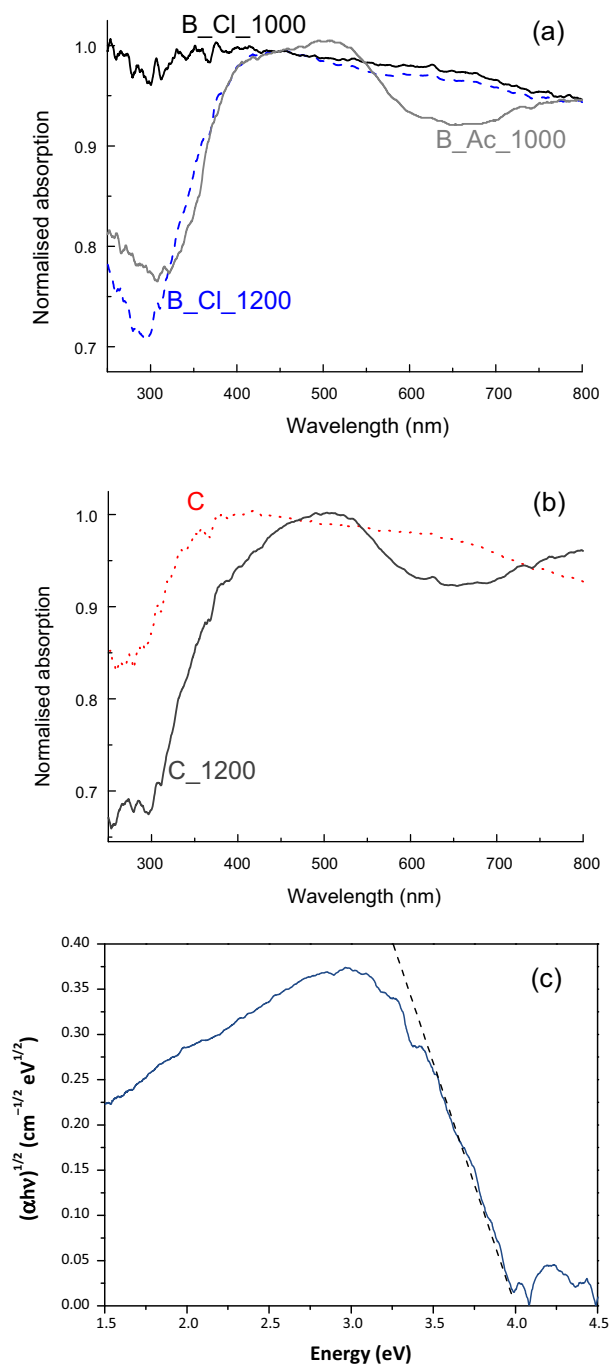

Fig. 2. UV spectra of (a) HAp samples of marine origin; (b) commercial HAp samples; (c) Example of a Tauc plot used to measure E$_g$, in this case for **B_Cl_1200**.

bouring OH groups being aligned in the opposite direction to form an antiferroelectric-like dipole structure (Fig. 1) [33,35,36]. For the phosphate groups, we considered the four different PO$_4$ environments which exist in the hexagonal HAp unit cell. Additionally, we considered a model with complex defects, consisting of both a full OH vacancy and an O vacancy from PO$_4$, simultaneously.

3. Results and Discussion

3.1. Experimental measurements

Fig. 2(a) and (b) show the measured UV spectra for the HAp samples of marine origin, and the commercial ones, respectively, while
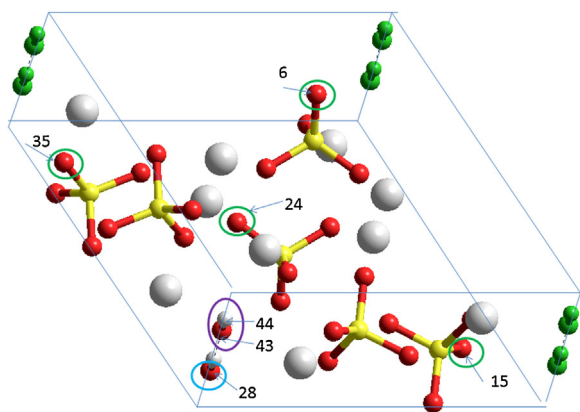
Fig. 3. Schematic of the atoms selected and deleted for modelling of various vacancy defects in the HAp hexagonal unit cell with 44 atoms. Indicated in the coloured circles are: (1) in blue − oxygen atom number 28 from an OH group for creation of an O vacancy in the OH-channel; (2) in purple − OH group with atom numbers 43 and 44 for creation of a complete OH vacancy; (3) in green − oxygen atoms with numbers 6, 15, 24, 35 from various differently positioned PO_4 groups corresponding to an O vacancy in PO_4 groups. The green atoms on the other three corners indicate other OH groups which to neighboring periodical unit cells. (For interpretation of the references to colour in this figure legend, the reader is referred to the web version of this article.)

Table 2 reports the band gap values calculated from the spectra. As already reported [16], the sample obtained from the bones treated with calcium acetate and annealed at 1000 °C (**B_Ac_1000**) shows a band gap of 3.4 eV. Moreover, some absorption in the visible region was also observed, between 500 and 650 nm. In fact, this sample had a sky blue colour. This phenomenon is known as "coring", and it is generally associated with an oxygen deficiency in the material [6].

When the bones were treated with calcium chloride (**B_Cl_1000**), they produced a relatively flat absorption spectrum, from which we were unable to observe/calculate the band gap of the material. Further annealing of this sample at 1200 °C, however, led to a major change in the UV absorption profile. A band gap value of 4.00 eV was calculated for **B_Cl_1200**, and a pale blue colour was observed in the sample.

The commercial HAp as provided, without any further treatment (**C**), had a very high band gap value of 4.92 eV. Annealing this at 1200 °C (**C_1200**) led to a decrease of the band gap to 3.95 eV; furthermore, absorption in the visible was also present, giving it a pale blue colour, similar to that seen for sample **B_Cl_1200**).

3.2. Computational results and modelling

The HAp unit cell model, showing the positions of all the vacancies used, is shown in Fig. 3. Here we indicate various types of O-vacancies in the HAp unit cell, as deviations from the initial stoichiometric hexagonal HAp structure:

1 An O vacancy in the OH group of an OH-channel structure (blue circle in Fig. 3).
2 A full OH vacancy from this OH-channel structure (purple circle in Fig. 3).
3 Various cases of O vacancies from different PO4 groups (green circles in Fig. 3).

The computed DOS for these examples are shown in Figs. 4–6, and the calculated data for their energy characteristics are presented in Table 3.

The computed DOS structures for initial stoichiometric hexagonal HAp, HAp with an O vacancy in the OH group, and a full OH group vacancy, are shown in Fig. 4. Fig. 5 depicts the DOS struc-
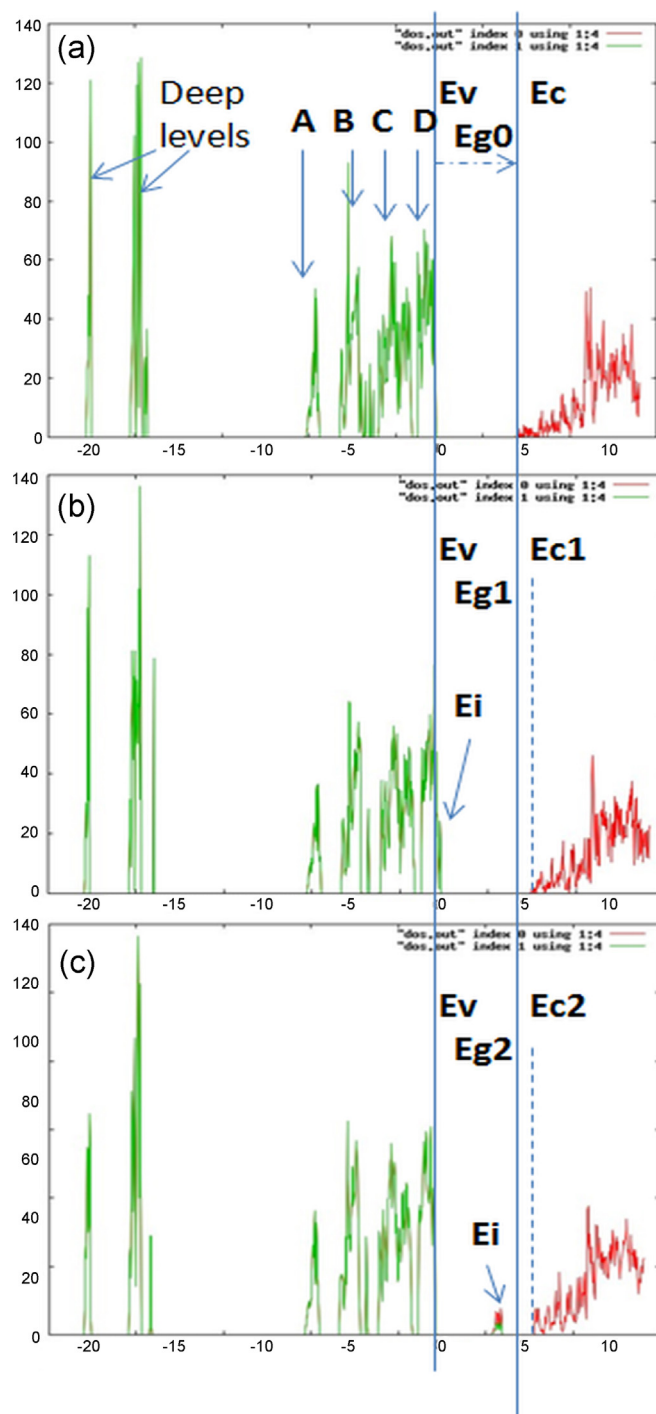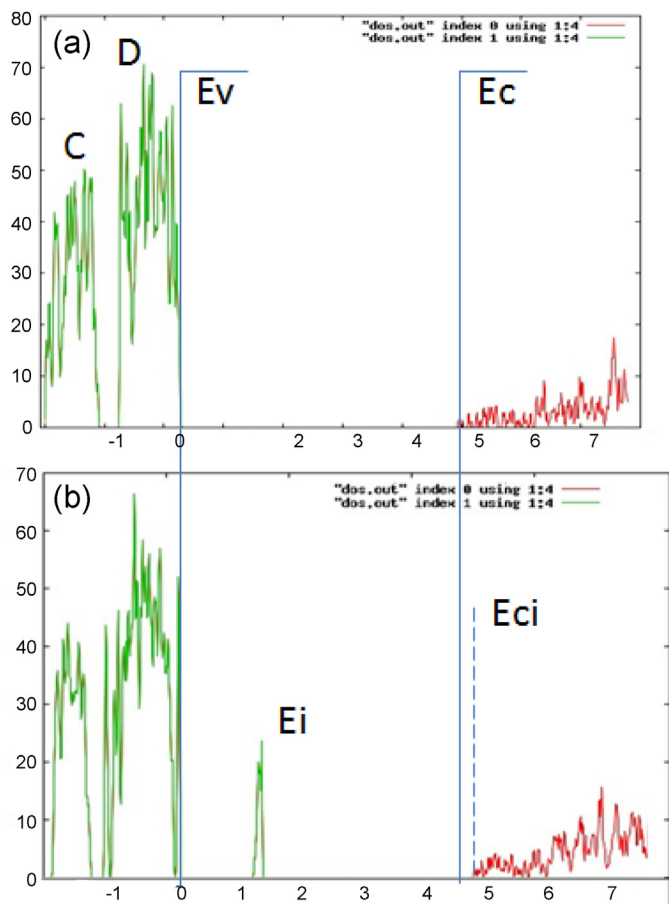

Fig. 4. Density of states for the central part around the forbidden band E_g in hexagonal HAp with a vacancy in OH groups: (a) for the stoichiometric hexagonal HAp structure; (b) with an O vacancy in the OH group from an OH-channel; (c) with complete OH vacancies. Green colours show energy levels occupied by electrons, red (to the right) shows unoccupied energy levels. Here A, B, C & D are the DOS for energy levels for HAp in the valence band, which are similar to previously reported works [23,38,39]. For the DOS peaks in the valence band: E_v = top of the valence band; E_c = bottom of the conductive band; $E_g = E_c - E_v$, the width of the forbidden band (this is E_g0 in the initial stoichiometric HAp); E_i is the energy of the additional local levels inside the forbidden zone, corresponding to defects.

Table 2
Sample preparation and corresponding measured band gap (E_g) value.

Sample name	Sample description	Heating temperature (°C)	Optical band gap, E_g (eV)
B_Ac_1000	Bones treated in calcium acetate	1000	3.44
B_Cl_1000	Bones treated in calcium chloride	1000	–
B_Cl_1200	Bones treated in calcium chloride	1200	4.00
C	Commercial sample	As supplied	4.92
C_1200	Commercial sample	1200	3.95

Fig. 5. DOS images for the central part around the forbidden band E_g in hexagonal HAp with a vacancy in the PO$_4$ group: (a) for stoichiometric initial HAp hexagonal, (b) with O vacancy in PO$_4$ group. Green colours show energy levels occupied by electrons, red (to the right) shows unoccupied energy levels. The following features are marked: C and D = the two upper peaks from the valence band; E_v = top of valence band; E_c = bottom of conductive band; $E_g = E_c - E_v$; E_i = DOS from energy levels inside forbidden band created by an O vacancy from the PO$_4$ group; E_{ci} = bottom of conductive band shifted by the HAp structure change after the O vacancy has arisen. This last change leads to the shift of the forbidden gap $E_g^* = E_{ci} - E_v$ (see Table 3 for details).

tures for an oxygen vacancy in one of the phosphate groups. The corresponding data are presented in Table 3.

Beyond these individual O or OH vacancies and their influences on the energetic and optical characteristics, we also investigated the more complex case of combined vacancies. We modelled the presence of two kinds of simultaneous vacancy in one HAp unit cell, with both an O vacancy from a PO$_4$ group and an entire OH vacancy from an OH-channel (Fig. 6 and Table 3). These entire OH vacancies often occur in HAP structures and samples, and can greatly influence their properties, especially for electronic states in forbidden bands and optical band [19,37].

From these modelling results, we can conclude the following:

1) An O vacancy from the OH group has a very small influence on the change of forbidden band gap E_g and optical spectral data. These data are in line with those previously published [19,38,39].
2) Entire OH vacancies create a deep and strong series of energy levels (narrow bands with several peaks) in the middle of the forbidden band. These energy levels (which are semi- occupied) play an important role in the trapping and recombination of electrons and holes, and create the optical spectral lines in the "green- red" visible regions.
3) An O vacancy in the PO$_4$ groups significantly changes the forbidden energy band gap, creating strong and fully-occupied energy levels inside forbidden band, with excited and absorbed energy corresponding to UVA and violet/blue optical wavelengths.
4) A simultaneous O vacancy in a PO$_4$ group in combination with an OH vacancy changes the forbidden energy band gap, and creates a series of energy levels inside forbidden band, which correspond to bands in the UV region, and peaks in the IR and visible red-orange-yellow wavelengths.

It is well known that in many cases of experimentally investigated HAp samples, the presence of OH vacancies was often observed in reasonably high concentration, which influences many properties of HAp [19,33,37]. Therefore, we can expect that HAp samples can contain both O vacancies from the PO$_4$ group and OH vacancies. Our modelling suggests that the presence in HAp of both types of vacancy simultaneously can create optical phenomena such as a shift in absorption from the violet-blue from just PO4 vacancies, to that in the red-orange-yellow region, between 500 and 650 nm. Such an effect has been observed in HAp after additional heating to 1000–1200 °C in some previous reports [23,37–39].

3.3. Comparison of modelled and measured data

The measured and calculated data are compared in Table 4. It can be seen that the measured values closely match calculated values for a variety of vacancy possibilities in the HAp structure.

The model indicated that an O-vacancy from the OH group resulted in the creation of a high forbidden band gap energy (E_g^*) of 5.05 eV (= 245 nm). The highest E_g we measured was in the as-supplied commercial sample **C** (a pure white sample), with a band gap of 4.92 eV; this suggests that this commercial HAp may contain intrinsic OH vacancies in its structure. However, this energy corresponds only to shortwave UVC light (100–280 nm, >4.43 eV), which is not present in sunlight as it is absorbed by the atmosphere and the ozone layer. This explains why such samples exhibit no photocatalytic activity under solar light. We were unable to measure any band gap at all for sample **B_Cl_1000**, also indicating this had no significant defects. In the stoichiometric initial HAp model with no defects, E_g was also calculated to be in this region, at 4.60 eV (270 nm).

However, for **B_Ac_1000**, which we had previously shown to be a good UV light photocatalyst, the measured band gap of 3.44 eV matches well with the modelled E_g^* values for oxygen defects in one of the four phosphate group environments, which gave values between 3.38-3.61 eV, with an average value of 3.58 eV. This

Computed data for hexagonal HAp with oxygen vacancies. The E_g^* values in the fifth column are the calculated shifted forbidden band gaps incurred by the vacancies, leading to enhanced absorption in UV and visible and ranges, and in some cases to photocatalytic activity. (AIMPRO optimized calculations, with accuracy $\pm 0.05 - 0.1$ eV).

Type of defect	Lattice parameters (Å)	Band gap, $E_g = E_c - E_v$ (eV)	E_i from E_v, $E_i - E_v$ (eV)	E_i from E_c $E_g^* = E_c - E_i$, Optical band (eV)	Optical band, E_g^* (nm)	Colour region of optical band
Initial HAP hex, P6₃	a=9.4732 c=6.9986	4.6	–	–	269.565	UVC
O vacancy in OH group	a=9.4732 a=9.4539 c=7.0028	5.15	Full occupied band0.1	5.05	245.545	UVC
OH vacancy	a=9.4732 a=9.4883 c=7.0018	5.49	½ occupied band = 3.11–3.82 with peaks at 3.40 3.53 3.66	Band = 2.38 −1.67 with peaks at 2.09 1.96 1.83	Band = 521.0 −742.5 with peaks at 593.3 632.65 677.6	Green-Red Orange Red Red
O6 vacancy in PO₄ group	a=9.45995 c=6.98844	4.7340	Full occupied peak 1.3465	3.3880	365.9980	UVA
O15 vacancy in PO₄ group	a=9.4630 c=6.9890	4.7680	Full occupied peak 1.3004	3.4677	357.5850	UVA
O24 vacancy in PO₄ group	a=9.47295 c=6.97822	4.5614*	Full occupied peak 0.955	3.6057	343.9095	UVA
O35 vacancy in PO₄ group	a=9.45808 c=6.989356	4.7346	Full occupied peak 1.3465	3.3881	365.9898	UVA
Average for O vacancy in PO₄ group	–	4.6995 ±0.13	–	3.5854 ±0.3005	358.3693 ±14.4683	UVA
O6 vacancy in PO4 and OH vacancy	a=9.47353 c=6.99394	5.4846	Full occupied peak = 1.2724 ½ −occupied band = 3.4663 − 3.9061 with peaks at 3.5540 3.6418 3.8173	4.2122 ½ −occ.band = 1.58 − 2.018 with peaks at 1.9306 1.8428 1.6673	294.537 785 − 614 642 670 742	UVB IR-Red-Orange Red Red Red
O35 vacancy in PO4 and OH vacancy	a=9.46857 c=6.99406	5.4907	Full occupied peak = 1.2738 ½ −occupied band = 3.3384 − 3.8216 with peaks at 3.5140 3.6458 3.7337	4.2169 ½ −occ.band = 1.67 − 2.15 with peaks at 1.977 1.845 1.757	294.057 743 − 576 627 672 706	UVB Red-Yellow Red Red Red

Table 4
Comparison of measured and modelled data for oxygen vacancies in HAp.

Sample measured	Measured band gap, E_g (eV)	Calculated band gap, E_g^* (eV)	Measured wavelength (nm)	Calculated wavelength (nm)	Vacancy modelled
C	4.92	5.05	252.0	245.5	O from OH
B_Ac_1000	3.44	3.47	360.4	357.3	O15 in PO4
B_Cl_1200	4.00	4.21	310.0	294.5	O6 in PO4 and whole OH
C_1200	3.95	4.21	313.9	294.5	O6 in PO4 and whole OH
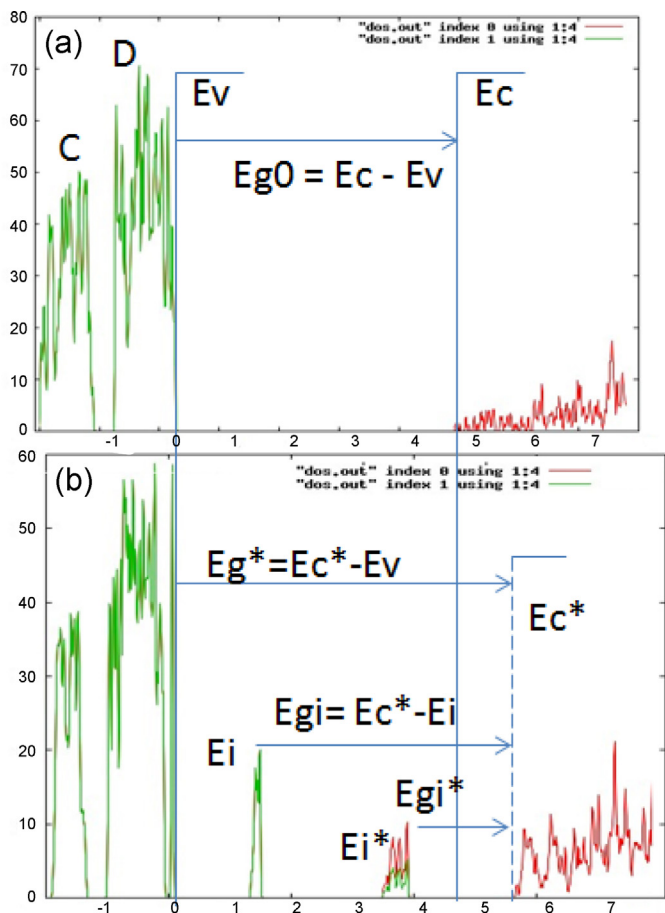
Fig. 6. DOS images for the central part around the forbidden band E_g in hexagonal HAp with simultaneous vacancies in the PO_4 and OH groups: (a) for stoichiometric initial hexagonal HAp; b) with simultaneous O vacancies in the PO_4 and OH groups. Green colours show energy levels occupied by electrons, red (to the right) shows unoccupied energy levels. The following features are marked: C and D = the two upper peaks from valence band; E_v = top of valence band; E_c = bottom of conductive band; $E_g0 = E_c − E_v$; E_i = DOS from energy level inside the forbidden band created by an O vacancy in the PO_4 group; E_i^* = DOS series of energy levels (narrow band) created from the OH vacancy; E_c^* = bottom of conductive band shifted by HAp structure change after O and OH vacancies have arisen. These last changes lead to the shift of the forbidden gap $E_g^* = E_c^* − E_v$, and forms several new lines in the optical spectrum due to the energy transfers $E_{gi} = E_c^* − E_i$ and $E_i^* = E_c^* − E_i^*$ (see Table 3 for details).

indicated that **B_Ac_1000** had an O vacancy in a phosphate group, most probably in the O15 or equivalent position, which had a calculated E_g^* of 3.47 eV (358 nm). This was attributed to the reducing effects of the organic acetate ligands burning out during calcination [16], resulting in the loss of oxygen stoichiometry. This band gap is well into the UVA region (315–400 nm), present in sunlight. This would explain why **B_Ac_1000** was an effective photocatalyst under UV light, both for the degradation of organic dye in solution and against microorganisms such as MRSA and *E. coli*. The fact that the sample was a blue colour also clearly indicates that this absorption also passes into the blue part of the visible spectrum, and it can be seen in Fig. 1 that the spectrum had already begun to decrease at ~450 nm.

Both samples heated at 1200 °C, **B_Cl_1200** and **C_1200**, exhibited similar, higher E_g values of around 4 eV, equivalent to ~310 nm, just inside the upper end of the UVB region (280–315 nm), and bordering on the UVA (Table 4). This is close to the calculated values for simultaneous mixed vacancies of both an oxygen atom in the phosphate groups (O6 or O35) and an entire OH group, which gave $E_g^* = 4.21$ eV. The fact that these values are slightly lower may indicate that the phosphate group vacancy is slightly favoured in these samples, shifting their active wavelength towards the UVA region. This suggests that the higher temperature of 1200 °C has encouraged vacancies to form, but in both phosphate groups and entire OH groups, whereas the organic reduction in **B_Ac_1000** led to vacancies in the phosphate groups only. It should be noted that both of these 1200 °C samples were also pale blue, indicating that they are also absorbing slightly in the visible region, as can be seen in Fig. 1. It should also be noted that the modelling suggests that these twin vacancies lead to a half-occupied band between 1.6-2.2 eV, causing significant energy peaks in the red and orange regions of the visible spectrum (Table 3).

Another interesting result from the modelling is that a vacancy of just an entire OH group by itself would lead to a wide band gap in the visible region of $E_g^* = 2.38 − 1.67$ eV (521–743 nm), in the green and red wavelengths. It would appear that we did not achieve such a vacancy in our materials, but if this type of specific vacancy could be induced, it could lead to a novel visible-light photocatalyst or optical material.

4. Conclusions

Density functional theory calculations and Density of States (DOS) modelling, was used to calculate the change of the optical band gap energy (E_g) upon introduction of various possible oxygen vacancies in the HAp lattice: O from PO_4, O from OH, simultaneous O from PO_4 + OH sites, and the loss of an entire OH group. The results were compared to measured data on both samples of marine origin and commercial HAp powders, and the modelled values were found to match the measurements very closely.

For the first time, the mechanisms and precise kinds of vacancies involved in the photocatalytic activity of HAp were proposed, and we suggest that:

1) In untreated non-photocatalytic HAp, if any vacancies exist, they are O atoms from the OH group, resulting in a band gap of ~5 eV in the UVC region. This wavelength of light is not present in solar light at the Earth's surface, being absorbed by the atmosphere, thus explaining why HAp usually displays no photocatalytic activity under sunlight.

2) In HAp containing acetate salts, reduction from the combustion of this organic component at 1000 °C led to oxygen deficiency in the phosphate groups, probably in the O15 position. This gives an E_g of ~3.45 eV, in the UVA region, which is present in sunlight, leading to the photocatalytic activity observed in this material under UV light. This HAp has a pale sky blue colour, attributed to oxygen vacancies, showing that it also absorbs slightly in the visible region.

3) Heating HAp with no organic component to 1200 °C led to mixed vacancies, of both an entire OH group, and oxygen from PO_4

groups (probably O6). This gave an intermediate E_g value of ~4 eV, on the boundary of the UVA-UVB regions. This material also had a pale blue colour, but less that of case 2) above, probably because less O vacancies were present. Modelling also predicts absorption peaks in the red-orange-yellow visible-light region with these combined vacancies.

4) Modelling predicts that a vacancy of just an entire OH group by itself would lead to a wide band gap in the green and red visible region, with an E_g in the range of 2.4 −1.6 eV (521–743 nm). If this type of specific vacancy could be induced, it could lead to a novel visible-light photocatalyst or optical material.

Acknowledgements

References

[1] S. Murgolo, F. Petronella, R. Ciannarella, R. Comparelli, A. Agostiano, M.L. Curri, G. Mascolo, UV and solar-based photocatalytic degradation of organic pollutants bu nao-sized TiO_2 grown on carbon nanotubes, Cat. Today 240 (2015) 114–124.
[2] D. Gu, H. Wu, Y. Zhu, B. Wang, Modified hierarchical TiO_2 NTs for enhanced gas phase photocatalytic activity, RCS Adv. 5 (2015) 57937–57942.
[3] H. Kisch, Semiconductor Photocatalysis: Principles and Applications, Wiley-VCH Verlag GmbH & Co, 2015.
[4] M. Tasbihi, M. Kete, A.M. Raichur, N.N. Tušar, U.L. Štangar, Photocatalytic degradation of gaseous toleuene by using immobilized titania/silica on aluminum sheets, Env. Sci. Poll. Res. 19 (2012) 3735–3742.
[5] D.M. Tobaldi, C. Piccirillo, R.C. Pullar, A.F. Gualtieri, M.P. Seabra, P.M.L. Castro, J.A. Labrincha, Silver-modified nano-titania as an antibacterial agent and photocatalyst, J. Phys. Chem. C 118 (2014) 4751–4766.
[6] C. Piccirillo, R.C. Pullar, E. Costa, A. Santos-Silva, M.M.E. Pintado, P.M.L. Castro, Hydroxyapatite-based materials of marine origin: a bioactivity and sintering study, Mater. Sci. Eng. C 51 (2015) 309–315.
[7] Y. Yan, X. Dong, X. Sun, X. Sun, J. Li, J. Shen, W. Han, X. Liu, L. Wang, Conversion of waste FGD gypsum into hydroxyapatite for removal of Pb^{2+} and Cd^{2+} from wastewater, J. Coll. Interf. Sci. 429 (2014) 68–76.
[8] J. Xie, X. Meng, Z. Zhou, P. Li, L. Yao, L. Bian, X. Gao, Y. Wei, Preparation of titania/hydroxyapatite (TiO2/HAp) composite photocatalyst with mosaic structure for degradation of pentachlorophenol, Mater. Lett. 110 (2013) 57–60.
[9] T. Giannakopoulou, N. Todorova, G. Romanos, T. Vaimakis, R. Dillert, D. Bahnemann, C. Trapalis, Composite hydroxyapatite/TiO2 materials for photocatalytic oxidation of NOx, Mater. Sci. Eng. B 177 (2012) 1046–1052.
[10] M. Wakamura, K. Hashimoto, T. Watanabe, Photocatalysis by calcium hydroxyapatite modified with Ti(IV): albumin decomposition and bactericidal effect, Langmuir 19 (2009) 3428–3431.
[11] A. Hu, M. Li, C. Chang, D. Mao, Preparation and characterization of a titanium-substituted hydroxyapatite photocatalyst, J. Molec. Cat. A 267 (2007) 79–85.
[12] K. Kandori, M. Oketani, Y. Sakita, M. Wakamura, FTIR studies on photocatalytic activity of Ti(IV)-doped calcium hydroxyapatite particles, J. Mol. Cat. A 360 (2012) 54–60.
[13] M. Tsukada, M. Wakamura, N. Yoshida, T. Watanabe, Band gap and photocatalytic properties of Ti-substituted hydroxyapatite: comparison with anatase-TiO_2, J. Molec. Cat. A 338 (2011) 18–23.
[14] H. Nishikawa, K. Omamiuda, Photocatalytic activity of hydroxyapatite for methyl mercaptane, J. Mol. Cat. A 179 (2002) 193–200.
[15] H. Nishikawa, A high active type of hydroxyapatite for photocatalytic decomposition of dimethyl sulphide under UV irradiation, J. Mol. Cat. A 207 (2004) 149–153.
[16] C. Piccirillo, C.W. Dunnill, R.C. Pullar, D.M. Tobaldi, J.A. Labrincha, I.P. Parkin, M.M. Pintado, P.M.L. Castro, Calcium phosphate-based materials of natural origin showing photocatalytic activity, J. Mater. Chem. A 1 (2013) 6452–6461.
[17] J.H. Shariffuddin, M.I. Jones, D.A. Patterson, Greener photocatalysts: hydroxyapatite derived from waste mussel shells for the photocatalytic degradation of a model azo dye wastewater, Chem. Eng. Res. Des. 91 (2013) 1693–1704.
[18] H. Nishikawa, Radical generation on hydroxyapatite by UV irradiation, Mater. Lett. 58 (2003) 14–16.
[19] V.S. Bystrov, J. Coutinho, A.V. Bystrova, R.C. Dekhtyar YuD. Pullar, A. Poronin, E. Palcevskis, A. Dindune, B. Alkan, C. Durucan, E.V. Paramonova, Computational study of hydroxyapatite structures, properties and defects, J. Phys. D: Appl. Phys. 48 (2015) 195302.
[20] J. Tauc, Optical properties and electronic structure of amorphous Ge and Si, Mater. Res. Bull. 3 (1968) 37–46.
[21] C. Piccirillo, R.C. Pullar, E. Costa, A. Santos-Silva, M.M.E. Pintado, P.M.L. Castro, Hydroxyapatite-based materials of marine origin: a bioactivity and sintering study, Mater. Sci. Eng. C 51 (2015) 309–315.
[22] A.S. Marfunin, Physics of Minerals and Inorganic Materials: An Introduction, Springer-Verlag, 1979.
[23] A. Slepko, A.A. Demkov, First-principles study of the biomineral hydroxyapatite, Phys. Rev. B 84 (2011) 134108.
[24] P. Hohenberg, M. Kohn, Inhomogeneous electron gas, Phys. Rev. B 136 (1964) 864.
[25] W. Kohn, L.J. Sham, Self-Consistent equations including exchange and correlation effects, Phys. Rev. A 140 (1965) 1133.
[26] J.P. Perdew, Y. Wang, Accurate and simple analytic representation of the electron-gas correlation energy, Phys. Rev. B 45 (1992) 13244.
[27] M.J. Rayson, P.R. Briddon, Rapid iterative method for electronic-structure eigenproblems using localised basis functions, Comp. Phys. Commun. 178 (2008) 128–134.
[28] AIMPRO, (2010). http://aimpro.ncl.ac.uk/ (Accessed February 2016).
[29] P.R. Briddon, M.J. Rayson, Accurate Kohn-Sham DFT with the speed of tight binding: current techniques and future directions in materials modeling, Phys. Status Solidi B 248 (2011) 1309–1318.
[30] C. Hartwigsen, S. Goedecker, J. Hutter, Relativistic separable dual-space Gaussian pseudopotentials from H to Rn, Phys. Rev. B 58 (1998) 3641.
[31] J.M. Hughes, M. Cameron, K.D. Crowley, Structural variations in natural F, OH, and Cl apatites, Am. Mineral. 74 (1989) 870–876.
[32] HyperChem, Tools for Molecular Modeling (release 7 8) Professional Edition, Hypercube, Inc., Gainesville, USA, 2002 (Accessed 02.16) http://www.hyper.com/?tabid=360.
[33] V.S. Bystrov, E.V. Paramonova, M.E.V. Costa, C. Santos, M. Almeida, S. Kopyl, A.V. Dekhtyar Yu Bystrova, E.I. Maevsky, R.C. Pullar, A.L. Kholkin, Computational study of the properties and surface interactions of hydroxyapatite, Ferroelectrics 449 (2013) 94–101.
[34] H.J. Monkhorst, J.D. Pack, Special points for Brillouin-zone integrations, Phys. Rev. B 13 (1976) 5188.
[35] M.I. Kay, R.A. Young, A.S. Posner, Crystal structure of hydroxyapatite, Nature 204 (1964) 1050–1052.
[36] V.S. Bystrov, E.V. Paramonova, A. Dekhtyar Yu Katashev, A. Karlov, N. Polyaka, A.V. Bystrova, A. Patmalnieks, A.L. Kholkin, Computational and experimental studies of size and shape related physical properties of hydroxyapatite nanoparticles, J. Phys.: Condens. Matter 23 (2011) 065302.
[37] D. Aronov, M. Chaikina, J. Haddad, A. Karlov, G. Mezinskis, L. Oster, I. Pavlovska, G. Rosenman, Electronic states spectroscopy of Hydroxyapatite ceramics, J. Mater. Sci: Mater. Med. 18 (2007) 865–870.
[38] P. Rulis, L. Ouyang, W.Y. Ching, Electronic structure and bonding in calcium apatite crystals: hydroxyapatite, fluoapatite, chlorapatite and bromapatite, Phys. Rev. B 70 (2004) 155104.
[39] K. Matsunaga, A. Kuwabara, First-principles study of vacancy formation in hydroxyapatite, Phys. Rev. B 75 (2007) 014102.